Available online at www.sciencedirect.com

ScienceDirect

Mendeleev Commun., 2021, **31**, 160–162

Mendeleev Communications

One step simultaneous electrochemical synthesis of NiO/multilayer graphene nanocomposite as an electrode material for high performance supercapacitors

Daria V. Chernysheva,[a] Igor N. Leontyev,*[b] Marina V. Avramenko,[b] Nikolay V. Lyanguzov,[b,c] Tatyana I. Grebenyuk[d] and Nina V. Smirnova[a]

[a] *Platov South Russian State Polytechnic University (NPI), 346428 Novocherkassk, Russian Federation*
[b] *Southern Federal University, 344090 Rostov-on-Don, Russian Federation. E-mail: i.leontiev@rambler.ru*
[c] *Southern Scientific Centre of the Russian Academy of Sciences, 344006 Rostov-on-Don, Russian Federation*
[d] *Don State Technical University, 344000 Rostov-on-Don, Russian Federation*

DOI: 10.1016/j.mencom.2021.03.005

A NiO/graphene nanocomposite has been prepared *via* one step electrochemical synthesis using simultaneous pulse alternating current dispersion of both Ni electrode and an electrode of thermally expanded graphite. Electron microscopy and Raman spectroscopy data reveals that the composite consists of graphene sheets with 2–5 layers having 0.5–2 μm size as well as NiO sheets with 200–250 nm dimensions comprising NiO nanoparticles of ~3.6 nm diameter. The electrochemical capacitance of the nanocomposite is 825 F g^{-1}, with retaining 89% of the initial value after 1000 operation cycles.

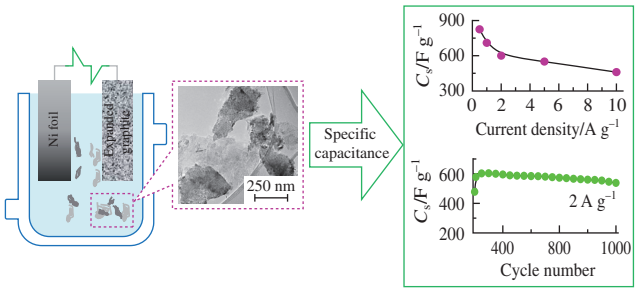

Keywords: graphene, transition metal oxide, nickel oxide, NiO nanoparticles, NiO/graphene, supercapacitor electrode material, electrochemical capacitance.

Over the last years, hybrid supercapacitors have emerged as promising energy storage devices. Transition metal oxides are typically used in these capacitors as electrode materials able to accumulate large amount of charge through Faradaic reactions on their surface. Nickel oxide represents particular interest[1] due to its high theoretical capacitance of 2584 F g^{-1} and good life-cycle stability in alkaline solutions. However, the conductivity of NiO does not fulfill the requirements for electrode materials, though it can be improved by embedding carbon additives[2] like ultradispersed soot, carbon nanotubes, nanofibers or graphene with formation of the corresponding NiO/C composites.[3,4] The graphene additive exhibits unique properties, such as high surface area, excellent flexibility, chemical inertness and good electrical conductivity.[5,6]

The capacitance of oxide-based composite electrode materials is known to depend on their microstructure, which in turn varies with the synthesis conditions, therefore, a powerful and simple method is needed for the fabrication of high-performance materials. For NiO/graphene nanocomposites, numerous synthetic routes are described,[4] for example the one step ball mill method.[7] However, typically the NiO nanocomposites are produced by multistep approaches, such as (i) microwave-assisted synthesis of void-induced graphene/wrapped NiO hybrids,[8] (ii) chemical bath deposition growth of NiO nanoflakes on a scaffold of ultrathin graphene/Ni foam hybrid,[9] (iii) electrodeposition of reduced graphene oxide (RGO) on Ni foam with subsequent deposition of $Ni(OH)_2$ and annealing to produce NiO nanowalls,[10] (iv) electrodeposition of a mixture of Ni^{2+}-decorated graphene oxide (GO) with the following oxidation of the obtained Ni metal to form NiO/GO composite,[11] (v) hydrothermal preparation of NiO with reduction of GO and NiO in water by hydrogen[12] or (vi) preparation of GO from graphite powder with subsequent solution-phase precipitation reaction between GO and $Ni(OH)_2$ followed by thermal reduction of the composite.[13] Two or more steps of the syntheses mentioned above can lead to accumulation of impurities in the products as well as to excessive consumption of energy and the need for expensive equipment for curing and drying the hydroxides *in vacuo* to transform them into oxides.

Direct electrochemical syntheses represent a convenient and available route for the production of ultradispersed powders, an example is alternating current (AC) electrolysis, which allows preparation of electrodes suitable as catalysts[14–16] as well as electrochemical energy storage materials.[17–19] In this work, we investigated NiO/multilayer graphene composite (NiO/MLG) produced *via* electrochemical dispersion with pulsed alternating current (EDPAC)[14,18,19] of a nickel electrode and an electrode of thermally expanded graphite. The EDPAC represents a simple one step method, which has been applied for fabrication of graphene support, Pt nanoparticles[14] and metal oxides. Here it has been used to synthesize NiO composite having both high capacity and stability for employment in supercapacitors.

Ni foil electrode as well as an electrode made of thermally expanded graphite with an area of 3 cm^2 each were immersed in 2 M solution of NaOH and connected to an AC source operating at a frequency of 50 Hz. Under these conditions, the Ni foil electrode was oxidized and both electrodes were dispersed in the electrolyte solution. The resulting suspension was filtered, the NiO/MLG powder was washed with distilled water and dried at 80 °C to a

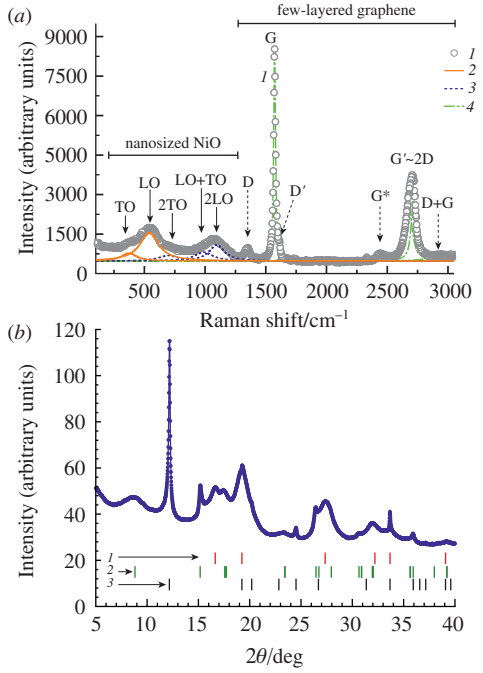

Figure 1 (*a*) Raman spectrum of (*1*) NiO/MLG composite, (*2*) first- and (*3*) second-order scattering features of nanosized NiO as well as (*4*) fingerprints of few-layered graphene (see the text for details). (*b*) XRD pattern of NiO/MLG composite, the vertical bars denote reflexes of (*1*) β-NiO, (*2*) β-$Ni(OH)_2$ and (*3*) graphite (see the text for details).

constant mass. The NiO content in NiO/MLG was found to be 40 wt% as determined from the weight loss of the Ni electrode and the total weight of the composite. The NiO/MLG sample was then investigated using Raman spectroscopy, powder X-ray diffraction (XRD), electron microscopy, cyclic voltammetry and chronopotentiometry.†

Figure 1(*a*) displays the Raman spectrum of NiO/MLG with numerous maxima, with the ones at 373, 540, 700, 987 and 1096 cm^{-1} being related to nanosized NiO, namely the first-order transversal and longitudinal optical (TO, LO) modes, mixed modes (LO+TO) as well as the second-order transversal and longitudinal optical (2TO, 2LO) vibrations. The G band of graphene at 1572 cm^{-1} represent an intrinsic one permitted by the Raman selection rules.[21,22] The lines at 1349 and 1612 cm^{-1} are associated with D and D′ modes, respectively, of plain C–C vibrations in the graphene lattice originated from defects either in the bulk or in the edges of the sheets. Other signatures in Figure 1(*a*), namely G*, G′~2D and D+G, represent superposition of D and D′ peaks with the G band as a result of double-resonance processes.[23,24] Note that the D to G peak intensity ratio equal to 0.056 reflects the density of defects within the graphene structure, and the greater the ratio is, the higher is the amount of defects. This parameter is typically used for estimation of imperfections in sp^2 carbon specimens.[23,24] The G′ band of graphene is composed of the two peaks at 2680 and 2714 cm^{-1}. Although its intensity is inferior to that of the G peak, the G′ band profile allows one to estimate the number of graphene layers as 3–5.[21–23] Note, that neither the two-magnon mode of nanosized NiO observed at 1490 cm^{-1} in works,[24,25] nor the fingerprints of $Ni(OH)_2$ expected at ~900–1000 cm^{-1} and ~3600 cm^{-1} according to article[26] manifest themselves in this spectrum presumably due to their overlapping with other high-intensity bands.

Figure 1(*b*) demonstrates the XRD powder pattern of NiO/MLG. Here, the broadened diffraction peaks (bars line *1*) are assigned to a face-centered cubic cell of β-NiO with a space group $Fm3m$ (JCPDS 75-0269). The reflexes of a rhombohedral cell $P\bar{3}m$ of β-$Ni(OH)_2$ (JCPDS 14-0117, bars line *2*) as well as the Bragg peaks attributed to hexagonal graphite with a space group $P6_3mc$ (JCPDS 75-1621, bars line *3*) are also observed. Note, that a visual inspection of the Raman spectrum in Figure 1(*a*) reveals no peaks of $Ni(OH)_2$, presumably as a result of its low concentration. Indeed, the area intensity ratio for the reflexes (100) and (200) from $Ni(OH)_2$ and NiO, respectively, is 0.07, which testifies to a low amount of the former in the composite. The average NiO nanoparticles size was evaluated by fitting the reflexes over a 2θ range of 14–22 deg using a WinPLOTR software.[27] Taking into account the values found by the fitting and after subtraction of the strain and instrumental contributions to the line broadening, the size was determined using the Scherrer equation[28] to be ~3.6 nm, which coincided well with TEM data (Figure 2). The unit cell parameter for NiO nanoparticles $a = 4.2632$ Å exceeds significantly the value for bulk NiO, which seems to originate from (i) intercalation of Na^+ ion into the NiO lattice during the synthesis and (ii) size effect, namely enlargement of the unit cell with a decrease in the nanoparticles size.[29]

The SEM and TEM images of NiO/MLG (see Figure 2) reveal a multilayer structure of graphene, which is in agreement with the Raman scattering data. The graphene sheet dimensions are

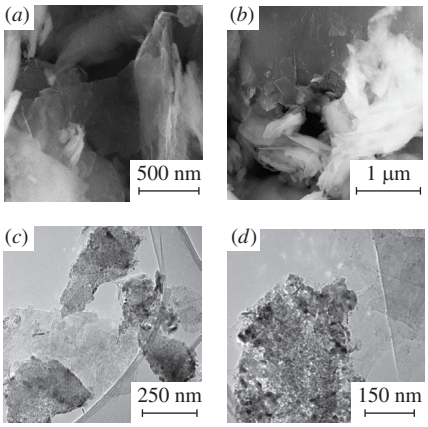

Figure 2 (*a*,*b*) SEM and (*c*,*d*) TEM images of freshly prepared NiO/MLG composite.

† Raman spectrum was recorded using a Renishaw spectrometer with a CCD detector at excitation by an Ar laser (λ = 514.5 nm) in the back-scattering mode in a wavelength range of 100–4000 cm^{-1}.

XRD measurements were carried out at the European Synchrotron Radiation Facility (France) using the Swiss–Norwegian Beam Lines (SNBL). Data were collected by a 2D Pilatus 2M plate detector (Dectris) in the Debye–Scherrer geometry (λ = 0.7121 Å). The instrumental resolution function was determined using LaB_6 as a reference sample provided by the National Institute for Standards and Technology (NIST). The data were processed using an SNBL ToolBox software.[20]

SEM and TEM images were obtained using Supra 25 (Carl Zeiss) and Titan (FEI) installations operated at 30 and 200 kV, respectively.

For electrochemical investigations, catalytic ink was fabricated by mixing NiO/MLG (14 mg), isopropyl alcohol (1 ml) and Nafion (0.0198 ml of 10 wt% solution). Cyclic voltammetry (CV) was performed using a PI-50Pro potentiostat/galvanostat (Elins, Russia) in a standard three electrode cell mode. Glassy carbon electrode with the air-dried catalytic ink (1.0 mg) as a working electrode was placed in 1 M aqueous solution of NaOH as an electrolyte and scanned at various rates up to 100 mV s^{-1}. Pt wire and Ag/AgCl were used as counter and reference electrodes, respectively. Galvanostatic charge–discharge (GCD) curves were recorded at current densities of 0.5, 1, 2, 5 and 10 A g^{-1} in a potential range of 0–0.5 V. Cycle-life/stability parameters were measured in the same E range. Specific capacitance C_s was evaluated from the GCD curves as $C_s = I\Delta t/m\Delta E$, where I was charge–discharge current (A), t represented the time of discharge (s), E was the discharge voltage (V) and m was the weight (g) of NiO as redox-dominant species in the working electrode.

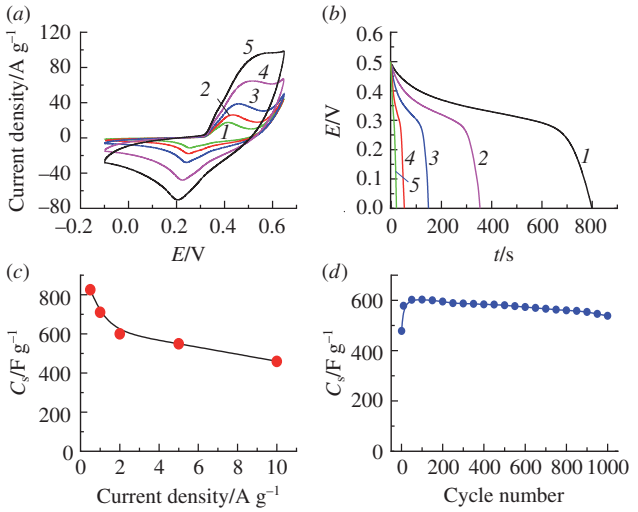

Figure 3 Electrochemical performance of NiO/MLG composite in 1 M aqueous solution of NaOH. (*a*) CV curves at different scan rates (mV s^{-1}): (*1*) 5, (*2*) 10, (*3*) 20, (*4*) 50 and (*5*) 100. (*b*) Galvanostatic discharge curves at various current densities (A g^{-1}): (*1*) 0.5, (*2*) 1, (*3*) 2, (*4*) 5 and (*5*) 10. (*c*) Specific capacitance C_s as a function of current density. (*d*) Cycling stability in the *E* range of 0–0.5 V at constant current density of 2 A g^{-1}.

estimated to be 0.5–2 μm. NiO exhibits a plate-like habit with linear plate dimensions of *ca.* 200–250 nm, with each plate comprising conglomerations of NiO nanoparticles of 2–5 nm size.

The electrochemical properties of NiO/MLG composite were investigated by CV at different scan rates [Figure 3(*a*)], where a quasi-reversible electron transfer occurred, therefore, the capacitance measured corresponded to the following Faradaic reactions involving NiO:

$$NiO + OH^- \rightleftharpoons NiOOH + e^-. \quad (1)$$

The CV curves of the NiO/MLG electrode remain similar with an increase in the scan rate, with anodic and cathodic peaks shifting towards the positive and negative potentials, respectively, primarily due to the electrode resistance. Furthermore, the elevation of current with an increase in the scan rate indicates a good rate capacity for the composite electrode at the high scan rate values [see Figure 3(*a*)].

The GCD behavior of the composite electrode was explored using chronopotentiometry at 0–0.5 V [Figure 3(*b*)]. The discharge curves consist of two sections, where a sudden potential drop is followed by a slow potential decay, the plateau represents the Faradaic reactions described by equation (1). The specific capacitance of the in-situ prepared NiO/MLG electrode material was evaluated to be 825, 710, 600, 550 and 460 F g^{-1} at discharge current densities of 0.5, 1, 2, 5 and 10 A g^{-1}, respectively [Figure 3(*c*)]. These values are much higher than those found for graphene-based NiO materials in works,[7–9,30,31] presumably due to the peculiar microstructure of the composite achieved in the one-pot fabrication of the graphene support and NiO. This type of structure ensures an interaction between the conducting and electrochemically active components in the bulk of the electrode and also can result in diffusion of electrolyte ions into pores, where further Faradaic reactions take place to improve the electrochemical energy storage.

The life-cycle stability as a parameter important for practical use was evaluated for the NiO/MLG electrode subjected to galvanostatic charge–discharge cycling at a current density of 2 A g^{-1} in a potential range of 0–0.5 V [Figure 3(*d*)]. The specific capacitance C_s increases from 478 to 603 F g^{-1} over the first 50 cycles due to the NiO activation. After 1000 cycles, C_s becomes 538 F g^{-1}, thus retaining ~89% of its maximum value and demonstrating sufficient stability after all the cycles. Thus, the synthesized NiO/multilayer graphene nanocomposite reveals promising characteristics as an electrode material for supercapacitors.

This work was supported by the Russian Science Foundation (grant no. 20-79-10063).

References

1 H. T. Tan, W. Sun, L. Wang and Q. Yan, *ChemNanoMat*, 2016, **2**, 562.
2 V. C. Lokhande, A. C. Lokhande, C. D. Lokhande, J. H. Kim and T. Ji, *J. Alloys Compd.*, 2016, **682**, 381.
3 Q. Ke and J. Wang, *J. Materiomics*, 2016, **2**, 37.
4 G. H. Jeong, S. Baek, S. Lee and S.-W. Kim, *Chem. – Asian J.*, 2016, **11**, 949.
5 M. Khan, M. N. Tahir, S. F. Adil, H. U. Khan, M. R. H. Siddiqui, A. A. Al-warthan and W. Tremel, *J. Mater. Chem. A*, 2015, **3**, 18753.
6 A. Jana, E. Scheer and S. Polarz, *Beilstein J. Nanotechnol.*, 2017, **8**, 688.
7 H. Kahimbi, S. B. Hong, M. Yang and B. G. Choi, *J. Electroanal. Chem.*, 2017, **786**, 14.
8 R. Kumar, R. K. Singh, R. Savu, P. K. Dubey, P. Kumar and S. A. Moshkalev, *RSC Adv.*, 2016, **6**, 26612.
9 C. Wu, S. Deng, H. Wang, Y. Sun, J. Liu and H. Yan, *ACS Appl. Mater. Interfaces*, 2014, **6**, 1106.
10 B. Zhao, T. Wang, L. Jiang, K. Zhang, M. M. F. Yuen, J.-B. Xu, X.-Z. Fu, R. Sun and C.-P. Wong, *Electrochim. Acta*, 2016, **192**, 205.
11 X. Hui, L. Qian, G. Harris, T. Wang and J. Che, *Mater. Des.*, 2016, **109**, 242.
12 W. Li, Y. Bu, H. Jin, J. Wang, W. Zhang, S. Wang and J. Wang, *Energy Fuels*, 2013, **27**, 6304.
13 J. Gui, J. Zhang, T. Liu, Y. Peng and J. Chang, *New J. Chem.*, 2017, **41**, 10695.
14 A. B. Kuriganova, I. N. Leontyev, M. V. Avramenko, Y. Popov, O. A. Maslova, O. Yu. Koval and N. V. Smirnova, *ChemistrySelect*, 2017, **2**, 6979.
15 A. B. Kuriganova, I. N. Leontyev, A. A. Ulyankina and N. V. Smirnova, *Mendeleev Commun.*, 2020, **30**, 663.
16 E. G. Kalinina and E. Yu. Pikalova, *Russ. Chem. Rev.*, 2019, **88**, 1179.
17 A. Kuriganova, D. Chernysheva, N. Faddeev, I. Leontyev, N. Smirnova and Y. Dobrovolskii, *Processes*, 2020, **8**, 712.
18 N. V. Smirnova, A. B. Kuriganova, D. V. Leont'eva, I. N. Leont'ev and A. S. Mikheikin, *Kinet. Catal.*, 2013, **54**, 255 (*Kinet. Katal.*, 2013, **54**, 265).
19 D. Chernysheva, C. Vlaic, I. Leontyev, L. Pudova, S. Ivanov, M. Avramenko, M. Allix, A. Rakhmatullin, O. Maslova, A. Bund and N. Smirnova, *Solid State Sci.*, 2018, **86**, 53.
20 V. Dyadkin, P. Pattison, V. Dmitriev and D. Chernyshov, *J. Synchrotron Radiat.*, 2016, **23**, 825.
21 A. C. Ferrari, J. C. Meyer, V. Scardaci, C. Casiraghi, M. Lazzeri, F. Mauri, S. Piscanec, D. Jiang, K. S. Novoselov, S. Roth and A. K. Geim, *Phys. Rev. Lett.*, 2006, **97**, 187401.
22 Y. Hernandez, V. Nicolosi, M. Lotya, F. M. Blighe, Z. Sun, S. De, I. T. McGovern, B. Holland, M. Byrne, Y. K. Gun'ko, J. J. Boland, P. Niraj, G. Duesberg, S. Krishnamurthy, R. Goodhue, J. Hutchison, V. Scardaci, A. C. Ferrari and J. N. Coleman, *Nat. Nanotechnol.*, 2008, **3**, 563.
23 R. Saito, M. Hofmann, G. Dresselhaus, A. Jorio and M. S. Dresselhaus, *Adv. Phys.*, 2011, **60**, 413.
24 R. E. Dietz, G. I. Parisot and A. E. Meixner, *Phys. Rev. B: Solid State*, 1971, **4**, 2302.
25 N. Mironova-Ulmane, A. Kuzmin, I. Steins, J. Grabis, I. Sildos and M. Pärs, *J. Phys.: Conf. Ser.*, 2007, **93**, 012039.
26 D. S. Hall, D. J. Lockwood, C. Bock and B. R. MacDougall, *Proc. R. Soc. A*, 2015, **471**, 20140792.
27 T. Roisnel and J. Rodríguez-Carvajal, *Mater. Sci. Forum*, 2001, **378–381**, 118.
28 P. Scherrer, *Nachr. Ges. Wiss. Goettingen, Math.-Phys. Kl.*, 1918, **2**, 98.
29 M. Fukuhara, *Phys. Lett. A*, 2003, **313**, 427.
30 X. Xia, J. Tu, Y. Mai, R. Chen, X. Wang, C. Gu and X. Zhao, *Chem. – Eur. J.*, 2011, **17**, 10898.
31 Y. Jiang, D. Chen, J. Song, Z. Jiao, Q. Ma, H. Zhang, L. Cheng, B. Zhao and Y. Chu, *Electrochim. Acta*, 2013, **91**, 173.

Received: 10th November 2020; Com. 20/6364